INRIA

INSTITUT NATIONAL DE RECHERCHE EN INFORMATIQUE ET EN AUTOMATIQUE

The behavior of two near-wall models for $k-\varepsilon$ prediction of stall

Ilya Abalakin and Bruno Koobus

N° 4075

Novembre 2000

THÈME 4

ISSN 0249-6399 ISRN INRIA/RR--4075--FR+ENG

INRIA
SOPHIA ANTIPOLIS

The behavior of two near-wall models for $k-\varepsilon$ prediction of stall

Ilya Abalakin* and Bruno Koobus†

Thème 4 — Simulation et optimisation
de systèmes complexes
Projet Sinus

Rapport de recherche n° 4075 — Novembre 2000 — 30 pages

Abstract: This study compares the application of several variants of the $k-\varepsilon$ model for the prediction of a stall around a two-body NLR airfoil. A Chen-Patel two-layer model and a Reichardt wall law combined or not with the Menter correction. The Reichardt wall-law does not give a good prediction of the stall, either with or without the Menter correction, although this second option is more accurate for non-detached flows. The stall is not predicted either by the original Chen-Patel two-layer model but well predicted if the Menter correction is added.

Key-words: Turbulence modelling, compressible, airfoil, high lift, stall

* IMM, Miuskaya sq., 4a, Moscow, Russia
† University of Montpellier 2, and INRIA

Unité de recherche INRIA Sophia Antipolis
2004, route des Lucioles, B.P. 93, 06902 Sophia Antipolis Cedex (France)
Téléphone : 04 92 38 77 77 - International : +33 4 92 38 77 77 — Fax : 04 92 38 77 65 - International : +33 4 92 38 77 65

Comportement de deux modèles proche paroi pour la prédiction d'un décrochement aérodynamique

Résumé : Cette étude compare les performances de deux versions du modèle $k-\epsilon$ sur la prédiction d'un décrochement aérodynamique autour d'un profil NLR a deux corps. On a considéré d'une part le modèle bi-couche de Chen-Patel et d'autre part une loi de paroi de Reichardt, les deux éventuellement combinés avec un terme correcteur dû à Menter. Le modèle de loi de paroi de Reichardt ne prédit pas le décrochement, avec ou sans la correction de Menter, bien que cette dernière correction apporte une meilleure prédiction des écoulement non décollés. Le décrochement n'est pas prédit par le modèle bi-couche sans la correction de Menter, cette correction en revanche donne accès à une bonne perdiction du décrochement.

Mots-clés : Modélisation de la turbulence, compressible, profil, hypersustentation, décrochement

1 Introduction

Aerodynamical studies of the external shape of an aircraft have been realized during the last three decades with a series of models with increasing complexity: small perturbation potential flow, full potential flow, Euler, Euler + Boundary layer, Reynolds-Averaged Navier-Stokes (RANS).

Each of these models has been useful at a stage of aircraft analysis and optimization. But today there is a need not only for analysing and understanding but also for predicting some complex phenomena such as separation around high-lift configurations, in order to design new efficient products.

This means that RANS models should be applied to complex geometries.

Now, we have to recall that RANS involve a lot of models with various complexities and predictivity.

We are talking about complexity first since it is a predominant factor in the choice of a model.

The Baldwin-Lomax model, for example, does not involve any extra differential equation, and this represents an important advantage in case of very expensive calculations on not so powerful computers; but this is not the most important issue today; the delay and engineer time is now more important, and from that point of view, the Baldwin-Lomax model is generally well dependant of a regular (preferably quasi-orthogonal) fine mesh near the no-slip boundary.

During a long time, it has been believed that $k - \varepsilon$ models were not accurate for external flows. In fact, the boundary treatment is so important that many calculation provided bad results due to numerical inaccuracies near the boundary.

Boundaries can be treated by two manners:

- *Low-Reynolds formulation.* Low-Reynolds formulations refer to the actual numerical simulation of the low-Reynolds quasi laminar part of the boundary layer. This option necessary the use of a fine mesh near the boundary, not only for the velocity, but also for closure variables, that show near the wall complex variation that must be well captured for the global accuracy although their own physical meaning is rather questionable. In order to get rid of the complex behavior of the closure variable ε, it is possible to match the two-equation model with a single-equation

one, applying only near the wall, and relying on a length scale, and this is the two-layer formulation.

- *High-Reynolds formulations.* Another way to deal with the small scales near the boundary is to approximately solve them with an analytic model. This is the wall law option, which allow calculations with much coarser meshes and therefore provide easier and more numerically finable results.

The two above versions assume that the near-wall flow attains an equilibrium. It is well-known that in most interesting cases, this does not hold. A very simple model, proposed by Menter, uses the Bradshaw law for taking into account non-equilibrium. This model can be easily introduced in the $k-\varepsilon$ model.

The purpose of this work is to compare the behaviors of a classical two-layer model, of a rather modern wall law proposed by Reichardt, and of their extensions involving the Menter correction.

2 Basic two-equation model

As a basic RANS model, the $k-\varepsilon$ model with two-layer formulation of Chen and Patel wall-adjacent turbulence is considered.

2.1 Conservation form of the system

The Reynolds averaged Navier-Stokes system relying to the $k-\varepsilon$ model is written in a conservative form as

$$\frac{\partial W}{\partial t}+\frac{\partial F(W)}{\partial x}+\frac{\partial G(W)}{\partial y}= \frac{1}{\mathrm{Re}}\left(\frac{\partial R(W)}{\partial x}+\frac{\partial S(W)}{\partial y}\right)+\frac{\partial \tilde{R}(W)}{\partial x}+\frac{\partial \tilde{S}(W)}{\partial y}+\Omega(W)$$

where :

- $W(x,y,t)$ is a functional array with values in $\mathbb{R}^6$, the components of which are the nondimensionalised conservative variables.

- $F(W)$ and $G(W)$ are the convective flux functions.
- $R(W)$, $S(W)$ are the laminar viscous fluxes. Re is the laminar Reynolds number obtained at the nondimensionalisation.
- $\tilde{R}(W)$, $\tilde{S}(W)$ are turbulent viscous flux functions.
- $\Omega(W)$ is the source term related to the $k-\varepsilon$ model.

Viscous turbulent stress also involves a diagonal term $2/3\rho k\mathcal{I}_d$ ($\mathcal{I}_d$ is the identity matrix) that is accounted through an adhoc variable change:

$$\begin{cases} p^{'} = p + \dfrac{2}{3}\rho k \\ E^{'} = E + \beta\rho k \quad \text{where} \quad \beta = -1 + \dfrac{2}{3(\gamma-1)} \end{cases}$$

with

$$\begin{cases} p = (\gamma-1)\rho C_v T \\ E = \rho C_v T + \dfrac{1}{2}\rho(u^2+v^2) + \rho k \end{cases}$$

where p is the pressure, E — the total energy per volume unit, ρ — the density, k — the turbulent kinetic energy, C_v holds of the specific heat for constant volume, T — the temperature, γ — the specific heat ratio assumed as constant ($\gamma = 1.4$ for a perfect gas) and u, v are mean flow velocity components. The relation between $E^{'}$ and $p^{'}$ is described by

$$p^{'} = (\gamma-1)\left(E^{'} - \frac{1}{2}\rho\left(u^2+v^2\right)\right)$$

Then convective fluxes turn to be:

$$F(W) = \begin{pmatrix} \rho u \\ \rho u^2 + p' \\ \rho uv \\ (E'+p')\,u \\ \rho uk \\ \rho u\varepsilon \end{pmatrix}, \quad G(W) = \begin{pmatrix} \rho v \\ \rho uv \\ \rho v^2 + p' \\ (E'+p')\,v = \\ \rho vk \\ \rho v\varepsilon \end{pmatrix}.$$

Laminar viscous fluxes are written as

$$R(W) = \begin{pmatrix} 0 \\ \tau_{xx} \\ \tau_{xy} \\ u\,\tau_{xx} + v\,\tau_{xy} + \dfrac{\gamma\,\mu}{\mathrm{Pr}}\dfrac{\partial e}{\partial x} + \beta\mu\,\dfrac{\partial k}{\partial x} \\ \mu\,\dfrac{\partial k}{\partial x} \\ \mu\,\dfrac{\partial \varepsilon}{\partial x} \end{pmatrix},$$

$$S(W) = \begin{pmatrix} 0 \\ \tau_{xy} \\ \tau_{yy} \\ u\,\tau_{xy} + v\,\tau_{yy} + \dfrac{\gamma\,\mu}{\mathrm{Pr}}\dfrac{\partial e}{\partial y} + \beta\mu\,\dfrac{\partial k}{\partial y} \\ \mu\,\dfrac{\partial k}{\partial y} \\ \mu\,\dfrac{\partial \varepsilon}{\partial y} \end{pmatrix}.$$

and turbulent viscous fluxes are defined as follows

$$\tilde{R}(W) = \begin{pmatrix} 0 \\ \tau^t_{xx} \\ \tau^t_{xy} \\ u\,\tau^t_{xx} + v\,\tau^t_{xy} + \dfrac{\gamma\,\mu_t}{\mathrm{Pr}_t}\dfrac{\partial e}{\partial x} + \dfrac{\mu_t}{\sigma_k}\dfrac{\partial k}{\partial x} + (1+\beta)\dfrac{\mu_t}{\sigma_k}\dfrac{\partial k}{\partial x} \\ \dfrac{\mu_t}{\sigma_k}\dfrac{\partial k}{\partial x} \\ \dfrac{\mu_t}{\sigma_\varepsilon}\dfrac{\partial \varepsilon}{\partial x} \end{pmatrix},$$

$$\tilde{S}(W) = \begin{pmatrix} 0 \\ \tau_{xy}^t \\ \tau_{yy}^t \\ u\,\tau_{xy}^t + v\,\tau_{yy}^t + \dfrac{\gamma\,\mu_t}{\mathrm{Pr}_t}\dfrac{\partial e}{\partial y} + \dfrac{\mu_t}{\sigma_k}\dfrac{\partial k}{\partial y} + (1+\beta)\dfrac{\mu_t}{\sigma_k}\dfrac{\partial k}{\partial y} \\ \dfrac{\mu_t}{\sigma_k}\dfrac{\partial k}{\partial y} \\ \dfrac{\mu_t}{\sigma_\varepsilon}\dfrac{\partial \varepsilon}{\partial y} \end{pmatrix},$$

where τ_{ij} and τ_{ij}^t represents respectively the laminar and turbulent stress tensors which are given by

$$\tau_{ij} = \mu\left(\frac{\partial u_i}{\partial x_j} + \frac{\partial u_j}{\partial x_i}\right) - \frac{2}{3}\mu\frac{\partial u_k}{\partial x_k}\delta_{ij} \quad , \quad u_1 = u \ , \ u_2 = v$$
$$\tau_{ij}^t = \mu_t\left(\frac{\partial u_i}{\partial x_j} + \frac{\partial u_j}{\partial x_i}\right) - \frac{2}{3}\mu_t\frac{\partial u_k}{\partial x_k}\delta_{ij}$$

Coefficient of turbulent viscosity μ_t is found from relation

$$\mu_t = c_\mu f_\mu \frac{\rho k^2}{\varepsilon}$$

The variation of nondimensional laminar viscosity coefficient μ as a function of a dimensional temperature T is defined by the Sutherland law

$$\begin{cases} \mu(T) = \mu_{ref}\dfrac{T}{T_{ref}} & \text{if } T \le 120\ K \\ \mu(T) = \mu(120)\left(\dfrac{T}{120}\right)^{1.5}\left(\dfrac{120+110}{T+110}\right) & \text{if } T \ge 120\ K \end{cases} \tag{1}$$

The source terms are

$$\Omega(W) = \begin{pmatrix} 0 \\ 0 \\ 0 \\ \beta\omega_k \\ \omega_k \\ \omega_\varepsilon \end{pmatrix}$$

The nondimensional parameters $\mathrm{Pr} = 0.725$, $\mathrm{Pr}_t = 0.86$ are respectively the laminar and turbulent Prandtl numbers and Reynolds number is $\mathrm{Re} = \rho_{ref} u_{ref} L_{ref} / \mu_{ref}$. Notations ρ_{ref}, u_{ref}, L_{ref} and μ_{ref} hold respectively for a reference density, velocity, length, viscosity. Finally, it is set

$$\begin{cases} \omega_k = -\rho\,\varepsilon + \mathcal{P} \\ \omega_\varepsilon = c_{\varepsilon_1} f_1 \dfrac{\varepsilon}{k}\mathcal{P} - c_{\varepsilon_2} f_2 \dfrac{\rho\,\varepsilon^2}{k} \end{cases}$$

where $\mathcal{P}$ denotes the production term of the turbulent kinetic energy which is given

$$\mathcal{P} = -\left(\frac{2}{3}\rho k \delta_{ij} - \mu_t\left(\frac{\partial u_i}{\partial x_j} + \frac{\partial u_j}{\partial x_i} - \frac{2}{3}\frac{\partial u_k}{\partial x_k}\delta_{ij}\right)\right)\frac{\partial u_i}{\partial x_j}$$

Constants c_μ, c_{ε_1}, c_{ε_2} empirically defined from experiments and f_1, f_2 and f_μ are damping functions. This constants and damping functions will be specified later.

2.2 Model for field far from wall

The high Reynolds simulation is carried out with the following issues:

$$\begin{cases} f_1 = 1 \\ f_2 = 1 \\ f_\mu = 1 \\ c_\mu = 0.09, \quad \sigma_k = 1.0, \quad \sigma_\varepsilon = 1.3, \quad c_{\varepsilon_1} = 1.44, \quad c_{\varepsilon_2} = 1.92. \end{cases}$$

2.3 Wall-adjacent model

A two-layer formulation introduced by Chen and Patel in 1988 [20] is chosen. Distance to wall will be accounted through the following quantity:

$$R_y = \frac{\sqrt{k}y}{\nu_w} \tag{2}$$

where ρ_w is the density at wall and ν_w is the kinematic coefficient of laminar viscosity at wall.

The one-equation low-Reynolds number model of Wolfshtein is used in the regions near the wall $R_y < 200$.

2.3.1 Region of high Reynolds number $R_y > 200$

In this region the standard $k-\varepsilon$ model is used:

$$\frac{D\ \rho k}{D\ t} = \frac{\partial}{\partial x}\left(\left(\mu + \frac{\mu_t}{\sigma_k}\right)\frac{\partial k}{\partial x}\right) + \frac{\partial}{\partial y}\left(\left(\mu + \frac{\mu_t}{\sigma_k}\right)\frac{\partial k}{\partial y}\right) - \rho\ \varepsilon + \mathcal{P}$$

$$\frac{D\ \rho\varepsilon}{D\ t} = \frac{\partial}{\partial x}\left(\left(\mu + \frac{\mu_t}{\sigma_\varepsilon}\right)\frac{\partial \varepsilon}{\partial x}\right) + \frac{\partial}{\partial y}\left(\left(\mu + \frac{\mu_t}{\sigma_\varepsilon}\right)\frac{\partial \varepsilon}{\partial y}\right) +$$

$$c_{\varepsilon_1}\frac{\varepsilon}{k}\mathcal{P} - c_{\varepsilon_2}\frac{\rho\varepsilon^2}{k}.$$

where $c_\mu = 0.09$, $\sigma_k = 1.0$, $\sigma_\varepsilon = 1.3$, $c_{\varepsilon_1} = 1.44$, $c_{\varepsilon_2} = 1.92$
and

$$\mu_t = \rho c_\mu \frac{k^2}{\varepsilon}\ .$$

2.3.2 Region of low Reynolds number $R_y < 200$

In this region only the kinetic energy k equation is solved while dissipation rate ε is derived from a mixing length l_ε:

$$\begin{cases} \dfrac{D\ \rho k}{D\ t} = \dfrac{\partial}{\partial x}\left(\left(\mu + \dfrac{\mu_t}{\sigma_k}\right)\dfrac{\partial k}{\partial x}\right) + \dfrac{\partial}{\partial y}\left(\left(\mu + \dfrac{\mu_t}{\sigma_k}\right)\dfrac{\partial k}{\partial y}\right) - \rho\ \varepsilon + \mathcal{P} \\ \\ \rho\varepsilon = \rho\dfrac{k^{\frac{3}{2}}}{l_\varepsilon} \end{cases}$$

where $\sigma_k = 1.0$ and the turbulent viscosity are given by :

$$\mu_t = c_\mu \rho\sqrt{k}\, l_\mu, \qquad \text{where} \qquad c_\mu = 0.09$$

The two mixing length l_μ and l_ε are defined by:

$$l_\mu = \kappa {c_\mu}^{-3/4} y f_\mu \quad \text{and} \quad l_\varepsilon = \kappa {c_\mu}^{-3/4} y f_\varepsilon \tag{3}$$

where f_μ and f_ε are two damping function:

$$f_\mu = 1 - \exp\left(\frac{-R_y}{A_\mu}\right) \quad \text{and} \quad f_\varepsilon = 1 - \exp\left(\frac{-R_y}{A_\varepsilon}\right) \tag{4}$$

with $\kappa = 0.4$, $A_\mu = 70$ and $A_\varepsilon = 2\kappa {c_\mu}^{-3/4}$.

2.3.3 Matching low- and high-Reynolds number regions

For $180 < R_y < 220$ it is assumed that the eddy viscosity varies linearly between the values given by the one-equation and standard $k-\varepsilon$ models:

$$\mu_t = \alpha \mu_t^{k-l} + (1-\alpha)\,\mu_t^{k-\varepsilon}$$

where

$$\alpha = \frac{220 - R_y}{40}. \tag{5}$$

2.4 The Menter correction

The Menter correction [19], is inspired by the one-equation model of Johnson and King [4] in which the turbulent stress tensor is assumed to be proportional to the turbulent kinetic energy in the logarithmic region of the turbulent boundary layer. Initially developed for being inserted in the $k-\omega$ model of Wilcox, the Menter correction redefines the turbulent viscosity in order to satisfy this proportionality

More precisely, this model relies on the Bradshaw relation [18]which defines the variation of the stress tensor as a function of the turbulent kinetic energy $\tau = \rho a k$ where a is a constant.

Production $\mathcal{P}$ and dissipation D terms write:

$$\mathcal{P} = \mu_t \left(\frac{\partial \bar{u}}{\partial y}\right)^2 \quad \text{and} \quad D = \rho\varepsilon$$

in which $\mathcal{P} = D$ whenever a local equilibrium holds. Starting from the definition of the local turbulent shear stress given by the Boussinesq assumption that the component of the turbulent stress $\tau = \mu_t \partial\bar{u}/\partial y$ and from the definition of the turbulent viscosity $\mu_t = c_\mu \rho k^2/\varepsilon$, we can re-write the turbulent stress tensor as follows

$$\tau = \rho\sqrt{c_\mu}\sqrt{\frac{\mathcal{P}}{D}}k$$

By identification, we derive a value for the constant a, equal to $\sqrt{c_\mu}$ in the case of a local equilibrium. Using the Bradshaw assumption, Menter redefines the

turbulent viscosity as follows:

$$\mu_t = \frac{\rho\sqrt{c_\mu}k}{\max\left(\dfrac{\varepsilon}{\sqrt{c_\mu}k}, \left|\dfrac{\partial u}{\partial y}\right| F\right)} \tag{6}$$

with

$$F = \tanh\left(\psi^2\right), \quad \psi = \max\left(2\frac{k^{\frac{3}{2}}}{y\varepsilon}, \frac{500\mu c_\mu k}{\rho\varepsilon y^2 \mathrm{Re}}\right)$$

The Menter model (6) allows to correct the turbulent viscosity when there is a local non-equilibrium between turbulence production $\mathcal{P}$ and dissipation D.
When the gradient of the normal velocity becomes weaker, i.e. out of the boundary layer, we recover the usual turbulent viscosity.
This model has been tested in combination with classical wall laws, see for example [17].

The adaptation of (6) to the present two-layer model is done, according to [5] as follows:

$$\mu_t = \frac{\rho\sqrt{c_\mu}k}{\max\left(\mathrm{cond}, \left|\dfrac{\partial u}{\partial y}\right| F\right)} \sqrt{\frac{f_\mu}{f_\varepsilon}} \tag{7}$$

with

$$\mathrm{cond} = \alpha\frac{\varepsilon}{\sqrt{c_\mu}k}\sqrt{\frac{f_\mu}{f_\varepsilon}} + (1-\alpha)\frac{\sqrt{k}}{\sqrt{c_\mu}l_y\sqrt{f_\mu f_\varepsilon}}, \quad \alpha = \min\left(\max\left(\frac{R_y - 200}{20}, 0\right), 1\right)$$

where α is given by (5), the correction functions f_μ and f_ε are defined in (4), and the length scale l_y is given by:

$$l_y = \kappa {c_\mu}^{-3/4} y. \tag{8}$$

2.5 The Reichardt wall law

Let u^+, y^+ be non-dimensional parameters defined as follows:

$$u^+ = \frac{\bar{u}}{u_f} \quad , \tag{9}$$

$$y^+ = \frac{\rho u_f}{\mu} y \quad . \tag{10}$$

The velocity u_f, also called friction velocity, is defined by means the shear stress tensor τ_w at the wall

$$u_f = \sqrt{\frac{\tau_w}{\rho}} \quad . \tag{11}$$

Reichardt wall-law allows to connect the laminar sub-layer flow with the logarithmic zone of the boundary layer. This wall law is described in details in [1]. It can be written as follows:

$$u^+ = \frac{1}{\kappa} ln\left(1 + \kappa y^+\right) + 7.8\left(1 - e^{-\frac{y^+}{11}} - \frac{y^+}{11} e^{-0.33y^+}\right) \quad . \tag{12}$$

This wall-law is suitable to describe the flow for an incompressible boundary layer; it can be employed to study slightly compressible boundary layers without appreciable errors.

Reichardt wall-law has the advantage of describing once for all the three types of behavior of the turbulent boundary layer, namely, the laminar layer, the logarithmic one and the intermediate layer, that is generally not described in usual wall laws. This is illustrated in Fig. 1; a logarithmic plot has been employed as usually , so that the logarithmic behavior is represented by a straight line on the plot. We note that the buffer zone is limited on bottom by value $y^+ = 4$ and on top by $y^+ = 32$.

Thus, Reichardt wall-law seems to predict with a good accuracy all the different parts of a boundary layer; moreover, it is sufficiently regular on his domain of definition and this represents an advantage for the numerical simulation.

This version of Reichardt wall-law is suitable to study flows with slight compressibility effects and small temperature gradients without appreciable errors.

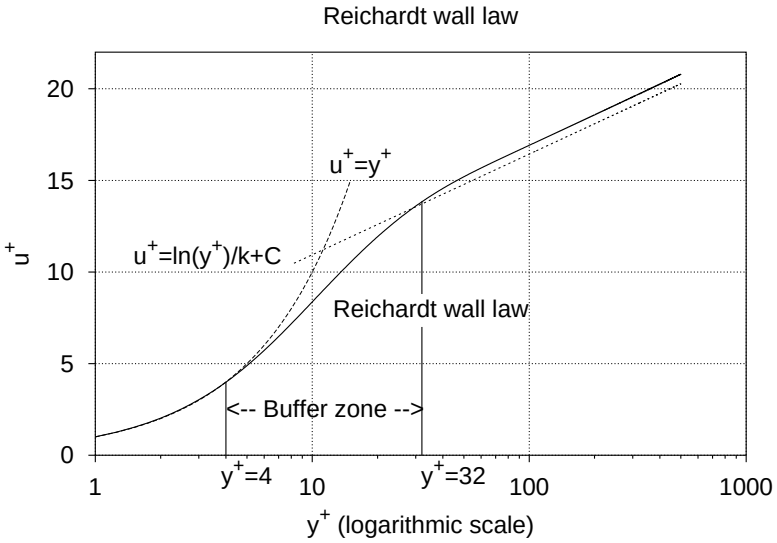

Figure 1: Comparison of Reichardt wall-law predictions with the laminar sublayer and outer layer approximated flows

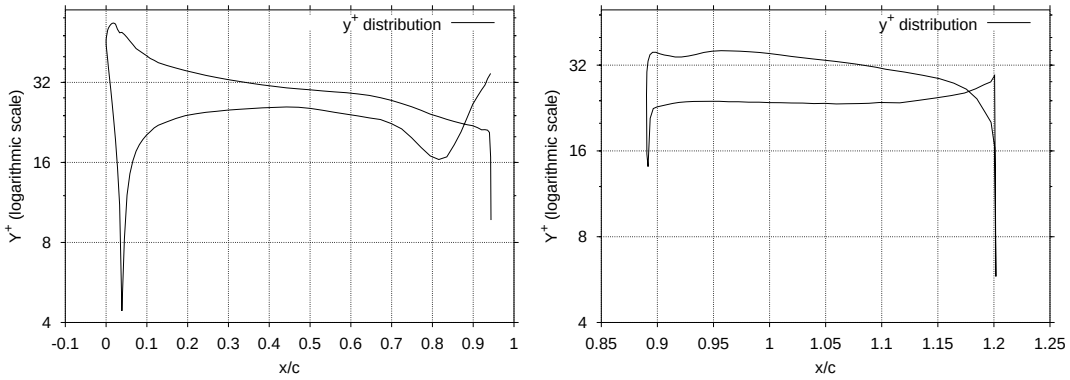

Figure 2: Distribution of the value y^+ along the main airfoil and flap

3 Numerical methodology for solving the flow problem

In this section, we give the main features of the numerical methods employed in this work for solving the flow problem given by the previous equation.

3.1 Spatial discretization

The spatial discretization of the fluid equations is based on a finite element/finite volume formulation on unstructured meshes. It combines a Roe upwind schemes for computing the convective fluxes, and the Galerkin centered method for evaluating the viscous terms. Second order space accuracy is achieved through a piecewise linear interpolation method based on the MUSCL (Monotonic Upwind Scheme for Conservation Laws) procedure [8, 9], and the slope limitation algorithm [10] can be employed in order to damp or eliminate the spurious oscillations that may occur in the vicinity of discontinuities. In the order to discretize accurately of flow equation on stretched meshes we use the cells introduced by Barth [11] and later by C. Viozat [12].

3.2 Time discretization

For solving accurately and efficiently the flow equations a first-order or second-order time-accurate implicit algorithm is employed. The time discretization is based on a second-order backward difference scheme. The nonlinear flow equations derived from the the time-discretization are solved by a defect-correction (Newton-like) method [13, 14].

4 Application to stall prediction

4.1 About the test case

The geometry is an two-component airfoil NLR 7301. This geometry was considered in an experiment by van den Berg [7]. The test-case chosen is well known as a test case of an European project, [15]. See [16] for a recent calculation. The Reynolds number is 2.51×10^6 and the Mach number is

0.185. A several angles of attack were taken from 0 degree to 16.1 degrees. Distributions of the pressure coefficient C_p are available, together with the lift coefficient. The lift coefficient shows a strong static stall for angles of attack more than 15 degrees.

Derived from the experiments, an abscissa of 0.03 was chosen for the shift from laminar to turbulent in both models. This means that the coefficient of the turbulent viscosity varies linearly beetween zero value (the laminar flow) and the value of μ_t defined by turbulent model

$$\mu_t^{all\ region} = \alpha_{trans}\mu_t \quad \text{where} \quad \alpha_{trans} = \min\left(1, \max\left(0, 1 - \frac{0.035 - x}{0.05}\right)\right)$$

Also the wall stress at wall is corrected as follows:

$$\tau_w \ = \ (1 - \alpha_{trans})\ \tau_w^L \ + \ \alpha_{trans}\ \tau_w^{RL}$$

where the value τ_w^L is proportional to tangential velocity and the value τ_w^{RL} is derived from Reichardt law (12).

A common mesh is used for both models. This is possible since the wall law model relies on an analytic layer thickness δ that is prescribed by user and not through the thickness of the first mesh row. In the sequel, we has observed that the best results were obtained with $\delta = 5 \times 10^{-4}$.

For this test case, the computed values of y^+ are depicted in Fig. 2. We note that these values are almost four times smaller than the middle point of the logarithmic region (see Fig. 1). Therefore, in many part of the wall the matching is applied in the upper region of the buffer zone.

5 Comparison before stall

A first series of calculations have been conducted in order to compare the pressure outputs provided by the two following options:

- the two layer model with Menter correction,
- the wall law model without Menter correction.

It appears that for medium angles of attack such as 6 degrees up to 10 degrees (Figs. 3-6), both model provide identically good pressure distribution.

However, for angles of 13 and 14 degrees (Figs. 7-10), a small deviation is observed on flap pressure distribution, while, airfoil distribution are hardly distinguishable. Since experiments are available for the 13.1 angle, we can note that the two-layer calculation is slightly better on upper side, slightly less good on lower side.

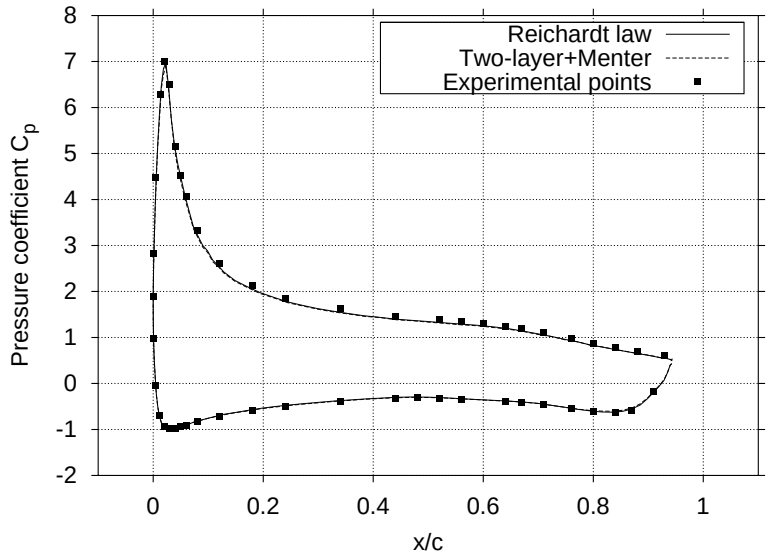

Figure 3: Distributions on NLR airfoil – 6°

6 Comparisons for stall conditions

Figs. 11-12 show the distribution Mach number for two types of flow — steady (angle of attack 13.1 degrees) and unsteady with the stall (16.1 degrees). We notice that for a steady flow both model (Reichardt law and two-layer) give approximately the same result. But for the unsteady flow obtained with the two-layer model with Menter correction we observe a long separation zone which starts at leading edge of the main airfoil (Fig. 11). At the same angle

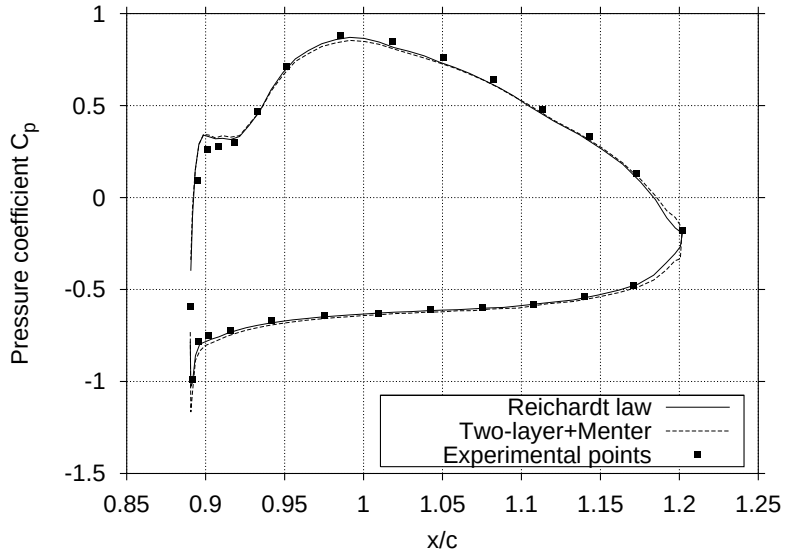

Figure 4: Distributions on flap – 6°

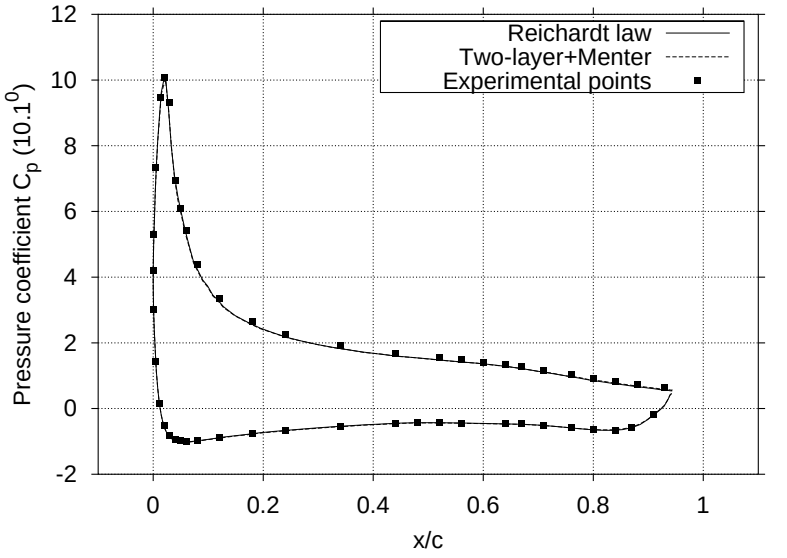

Figure 5: Distributions on NLR airfoil – 10.1°

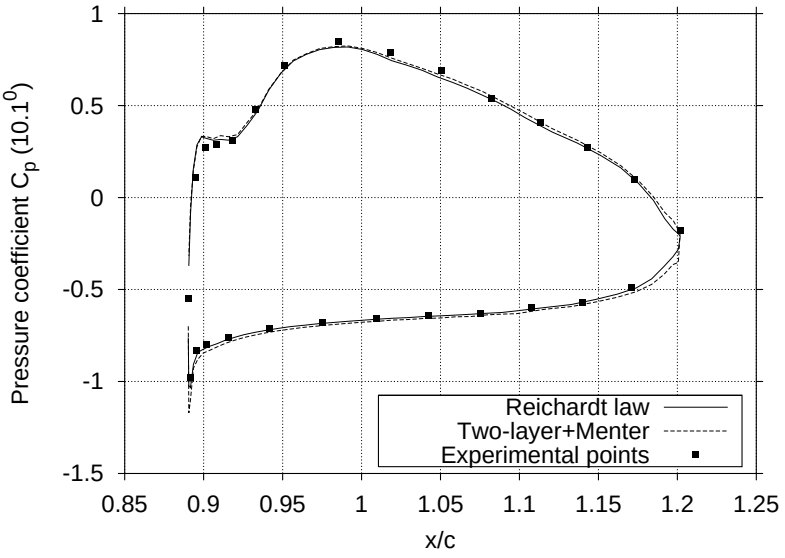

Figure 6: Distributions on flap – 10.1°

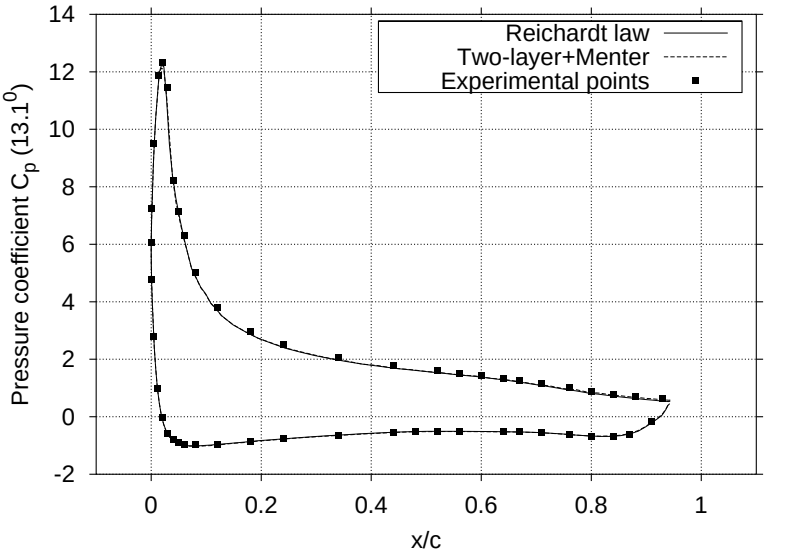

Figure 7: Distributions on NLR airfoil – 13.1°

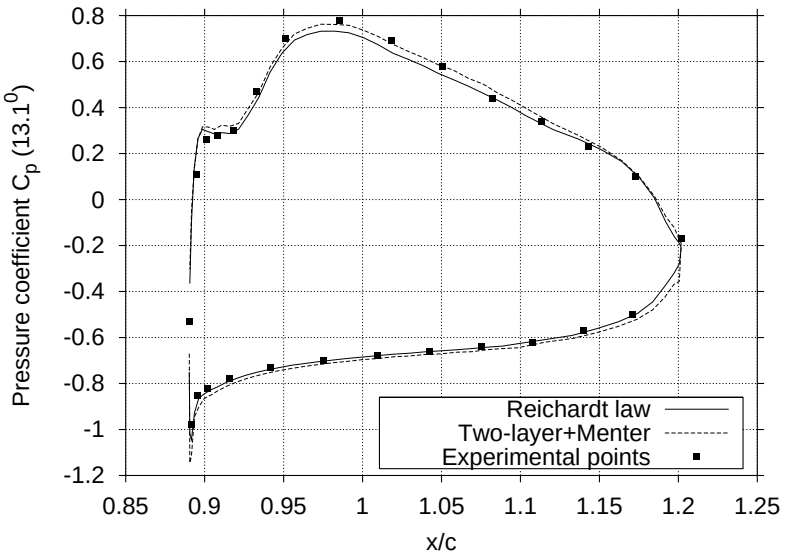

Figure 8: Distributions on flap – 13.1°

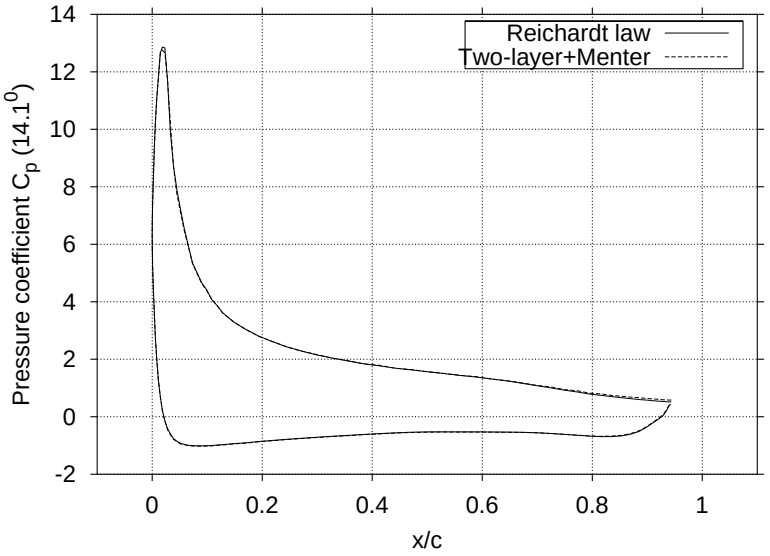

Figure 9: Distributions on NLR airfoil – 14.1°

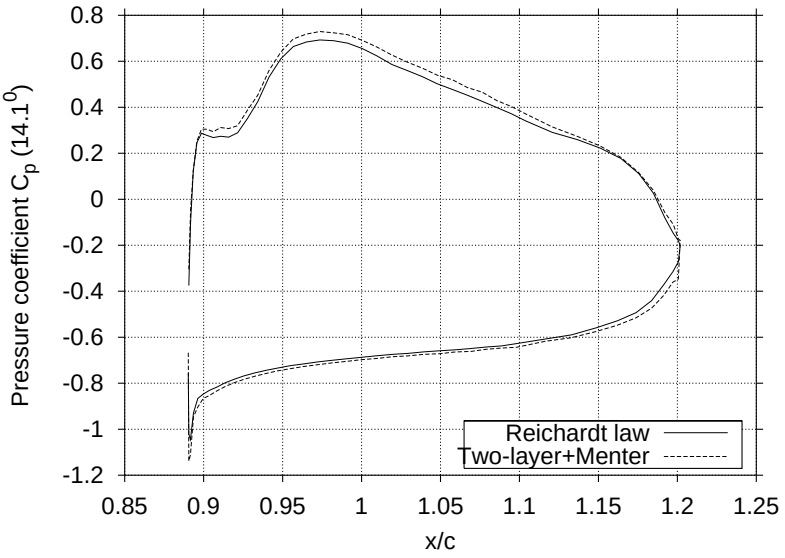

Figure 10: Distributions on flap – 14.1°

of attack, Reichardt's wall law predicts only a steady solution without separation(Fig. 12).

At 15.1 degrees, the Reichardt model gives a fully attached flow with high lift. Pressure distributions are very similar to the previous ones, with, apparently an even better lift. In contrast, the two-layer model give an unsteady flow, with separation, and pressure distributions show a dramatically compressed pressure curve, especially for the main airfoil (Fig. 13-14)

For 16.1 degrees, the Reichardt model gives still lift increment, and still similar curves. We depict also an instantaneous result for the two-layer model, that is a little difficult to exploit because of unsteadiness (Fig. 15-16).

The lift coefficient measured on all the above computations is depicted in Figs. 17. For unsteady flows, we use a time averaged lift coefficient. It appears that the good prediction of the stall given by the two-layer model is completely missed by the Reichardt law model.

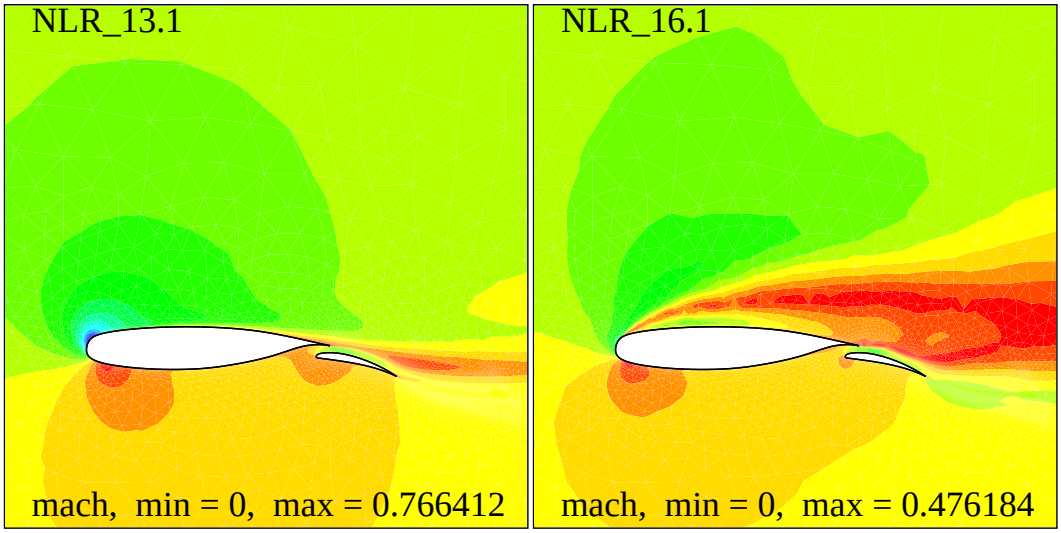

Figure 11: Stall prediction for a NLR airfoil with the two-layer model and Menter correction (courtesy of J. Francescatto)

Angle of attack	Two-layer model	Rechardt law	Reichardt law with Menter	Experimental data
10.1	2.845	2.838	2.853	2.877
13.1	3.120	3.091	3.129	3.141
14.1	3.166	3.141	3.193	3.197

Table 1: Comparison lift coefficients are computed with two-layer model with Menter correction, Reichardt law, Reichardt law with Menter and experimental results

6.1 Reichardt wall law and Menter correction

This section is focused on the combination of Reichardt wall law and Menter correction.

Using the Menter modification in combination with the Reichardt law model allows to achieve more accurate results in prediction of steady flow.

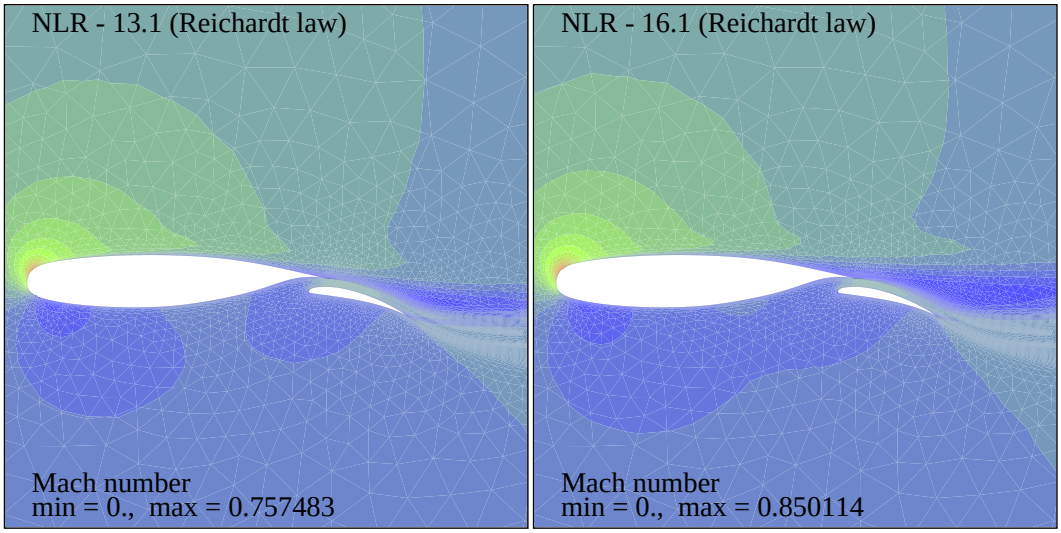

Figure 12: Flow prediction for a NLR airfoil with the Reichardt law, angle of attack — 13.1 and 16.1 degrees

In Table 1 we can see the improvement of the lift coefficient value in comparison with Reichardt law computations. We also observe that the change carried by introducing the Menter correction is a little disappointing for an angle of 13.1 degrees.

A comparison of the pressure coefficient obtained by the Reichardt wall law with Menter correction and the two-layer model also with Menter modification depicted in Figs. 18-19. It appears that the results obtained by the Reichardt wall law model with or without Menter correction are quite the same.

Conversly, at an angle of attack of 15.1 degrees, the lift coefficient finally stabilize at 1.62, a value that is of comparable quality to that of the two-layer computation (see Fig. 17)

7 Conclusions

In this study, two models representing two families have been compared for a test case representative of stall prediction problems.

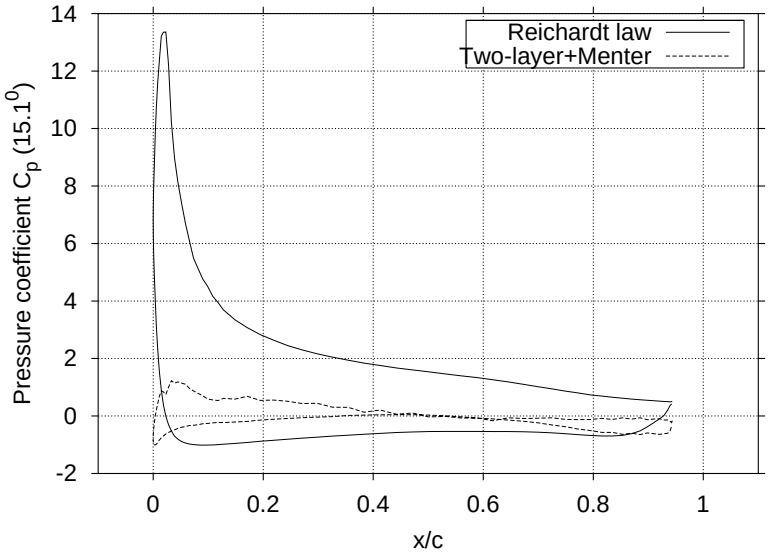

Figure 13: Distributions on NLR airfoil – 15.1°

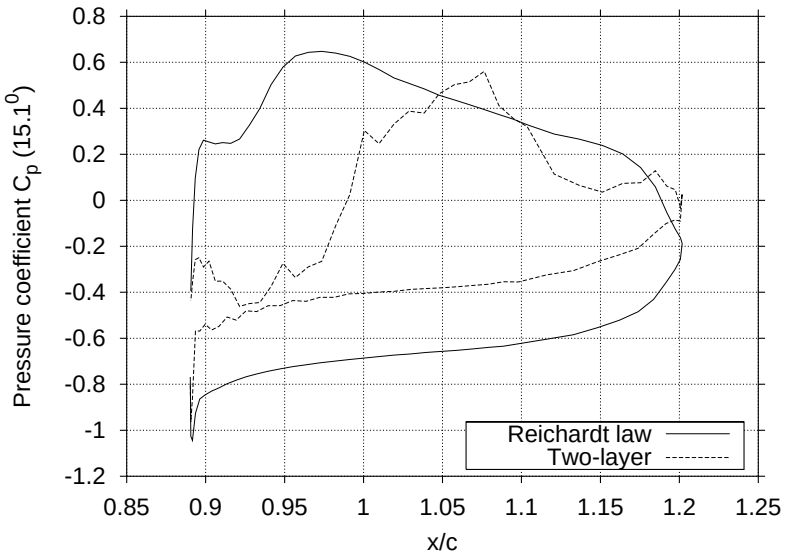

Figure 14: Distributions on flap – 15.1°

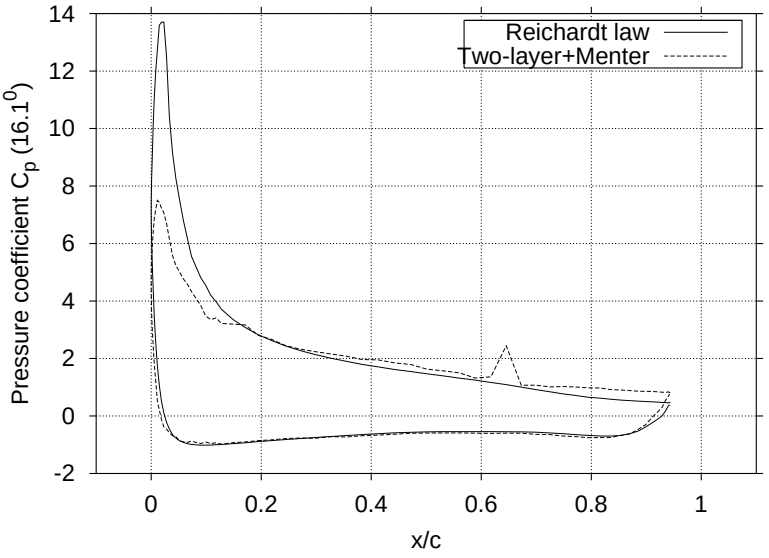

Figure 15: Distributions on NLR airfoil – 16.1°

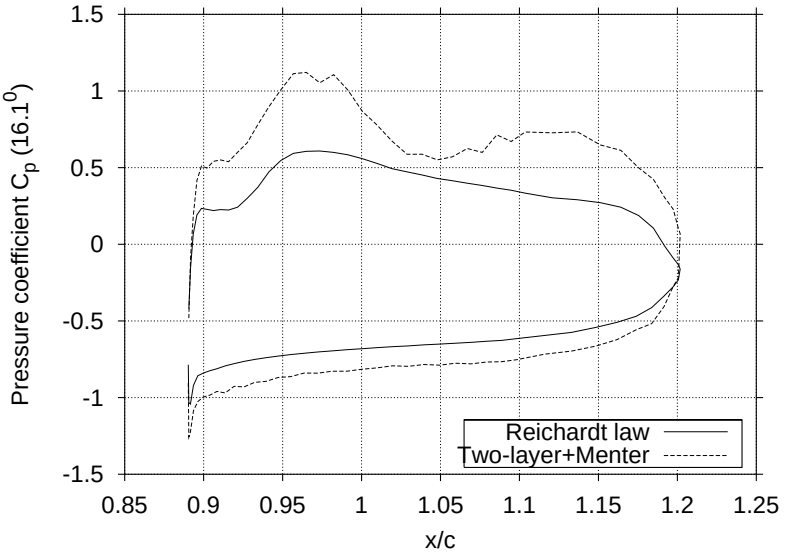

Figure 16: Distributions on flap – 16.1°

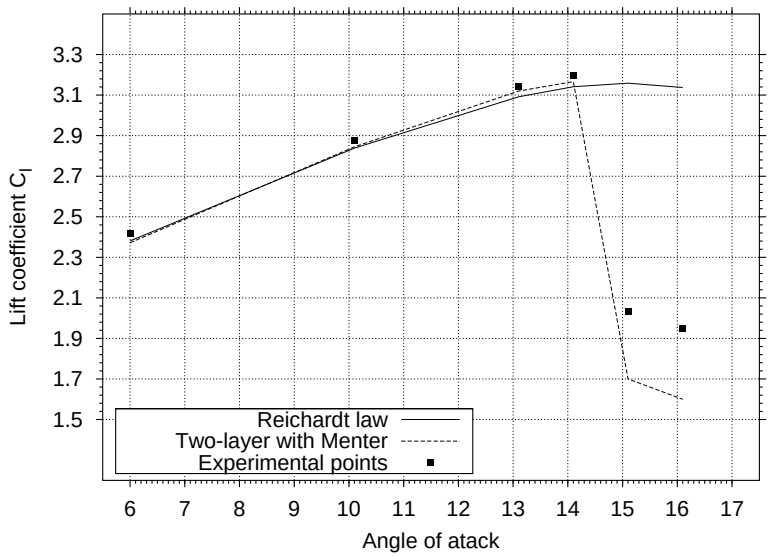

Figure 17: Lift coefficient for different angles of attack

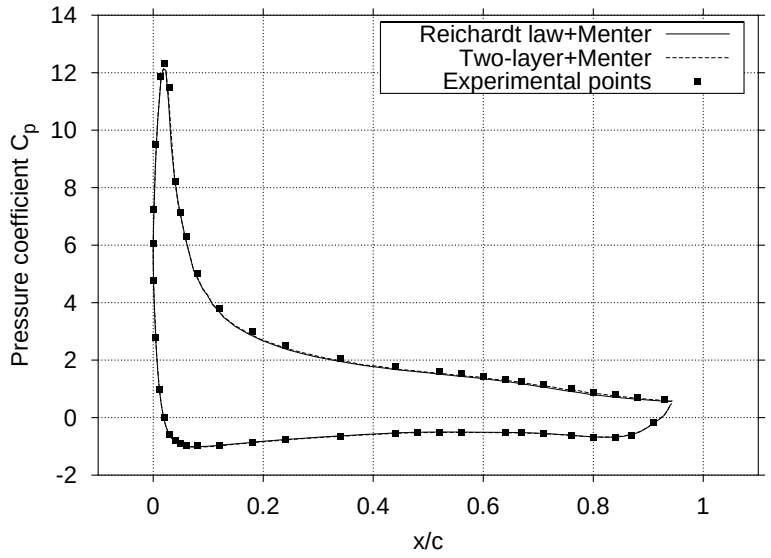

Figure 18: Distributions of pressure coefficient on the main airfoil, angle of attack — 13.1 degrees

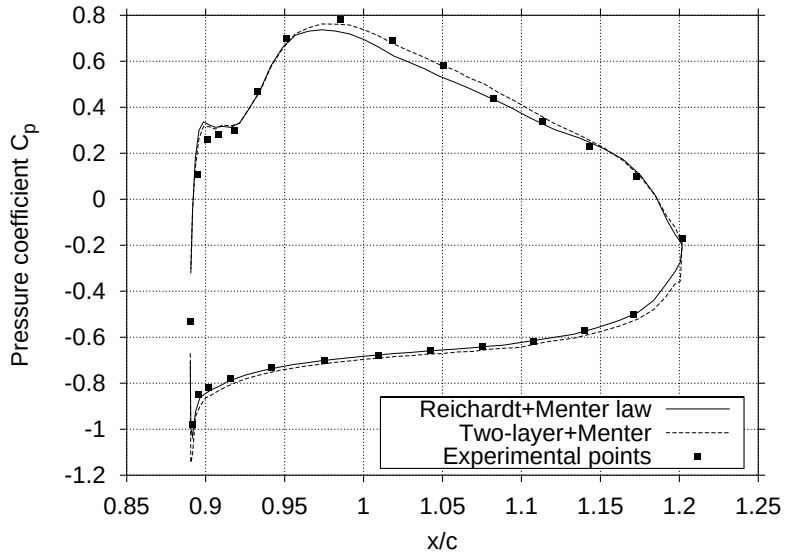

Figure 19: Distributions of pressure coefficient on flap, angle of attack — 13.1 degrees

The Reichardt wall law is a modern wall law allowing a good resolution of the boundary layer for a large choice of boundary layer thickness. It does not need a very fine mesh at wall and can be in practice 6 to 10 times less expensive than a low-Reynolds treatment.

The two-layer Chen-Patel model is a low-Reynolds treatment of medium cost, since it is rather robust and does not involve the resolution of the ε variable at wall. It needs however a fine mesh at wall for the resolution of k and of mean flow variables.

Computations have been performed for the both models with the same mesh, a fine one, in order to avoid numerical inaccuracies. Both series of calculation have shown robustness, and comparable computational cost.

The Reichardt wall law produced best results with a small boundary layer thickness, corresponding to the buffer zone; it has been examined with this option. It behaves well for angles of attack less than the experimental stall one, but the stall is not predicted.

The Chen-Patel model presented here behaves like (or slightly better than) the standard wall-law for small angles of attack, with an underprediction of the lift. The stall is not predicted either.

If we introduce the Menter correction in both models, it carries minor modifications to the Reichardt law before stall, and not yet a good stall angle prediction.

It carries a slightly better improvement to the two-layer model for angles lower than stall; maybe this remark tends to prove that our mesh was not still enough good for the two-layer model. However, introducing the Menter correction in to the two-layer correction allows a good prediction of stall angle.

8 Acknowledgements

The NLR airfoil mesh was provided by Vittorio Selmin (Alenia-Turin). We thank Jérôme Francescatto for providing the two-layer software.

References

[1] J.O. Hinze: *Turbulence*, McGraw-Hill, New York, (1959).

[2] F.R. Menter, "Zonal Two-Equation $k-w$ Turbulence Models for Aerodynamic Flows", *AIAA Paper 93-2906*, 1993.

[3] J.A. Ekarerinaris, F.R. Menter, "Computation of Separated and Unsteady Flows with One- and Two- Equation Turbulence Models", *AIAA Paper 94-0190*, 1994.

[4] D.A. Johnson, L.S. King, "A Mathematically Simple Turbulence Closure Model for Attached and Separated Turbulent Boundary Layers", *AIAA Journal*, Vol. 23, pp. 1684-1692, 1985.

[5] J. Francescatto, "Méthodes multigrilles par agglomération directionnelle pour le calcul d'écoulements turbulents", *Thèse de l'Université de Nice Sophia-Antipolis*, 1998.

[6] P. G. Huang, P. Bradshaw and T. J. Coakley, "Turbulence Models for Compressible Boundary Layers", *AIAA Journal*, Vol. 32, April 1994.

[7] B. Van den Berg, "Boundary layer measurements on a two-dimensional wing with flap", National Aerospace Laboratory, NLR TR 79009 U, Amsterdam, The Netherlands, 1979.

[8] B. Van Leer, "Towards the Ultimate Conservative Difference Scheme V: a Second-Order Sequel to Godunov's Method", *J. Comp. Phys.*, Vol. 32, pp. 361–370, 1979.

[9] A. Dervieux, "Steady Euler Simulations Using Unstructured Meshes", *Von Karman Institute Lecture Series*, 1985.

[10] G. D. Van Albada, B. Van Leer et W. W. Roberts, "A Comparative Study of Computational Methods in Cosmic Gas Dynamics", *Astron. Astrophys.*, Vol.108, pp. 76–84, 1982.

[11] T.J. Barth, "Aspects of unstructured grids and finite-volume solvers for the Euler and Navier-Stokes equations", *Von Karman Institute Lecture Series*, 1994.

[12] C. Viozat, "Calcul d'écoulements stationnaires et instationnaires à petit nombre de mach, et en maillages ètirès", *Thèse de l'Université de Nice Sophia-Antipolis*, 1998.

[13] K. Bohmer, P. Hemker, et H. Stetter, "The Defect Correction Approach", *Comput. Supp.*, Vol. 5, pp. 1–32, 1984.

[14] R. Martin et H. Guillard, "A Second-Order Defect Correction Scheme for Unsteady Problems", *Comput. and Fluids*, Vol. 25, pp. 9–27, 1996.

[15] W. Haase, E. Chaput, E. Elsholz, M.A. Leschziner and U. R. Mueller (editors), ECARP-European Computational Aerodynamics Research Project : Validation of CFD codes and Assessment of Turbulence Models, *Notes on Numerical Fluid Mechanics*, 58, Vieweg Verlag, 1996.

[16] D.G. Koubogiannis and K.C. Giannakoglou, "Implemantation and assessment of low-Reynolds turbulence models for airfoil flows on unstructured grids", ECCOMAS'2000, Barcelona, Spain, to appear

[17] G. Carré, "Résolution d'écoulement turbulents compressibles stationnaires par méthodes multigrilles", *Thèse de l'Université de Nice Sophia-Antipolis*, 1995.

[18] Huang P.G., Bradshaw P., Coakley T.J., "Turbulence Models for Compressible Boundary Layers"- *AIAA Journal*, Vol 32, pp. 735–740, 1994.

[19] Menter F.R., "Zonal Two-equation $k-\omega$ Turbulence Models for Aerodynamic Flows", *AIAA 93-2906*, 1993.

[20] H.C. Chen, V.C. Patel, "Near-Wall Turbulence Models for Complex Flows Including Separation", *AIAA Journal*, Vol. 26, pp. 641–648, 1988.

Unité de recherche INRIA Sophia Antipolis
2004, route des Lucioles - B.P. 93 - 06902 Sophia Antipolis Cedex (France)

Unité de recherche INRIA Lorraine : Technopôle de Nancy-Brabois - Campus scientifique
615, rue du Jardin Botanique - B.P. 101 - 54602 Villers lès Nancy Cedex (France)
Unité de recherche INRIA Rennes : IRISA, Campus universitaire de Beaulieu - 35042 Rennes Cedex (France)
Unité de recherche INRIA Rhône-Alpes : 655, avenue de l'Europe - 38330 Montbonnot St Martin (France)
Unité de recherche INRIA Rocquencourt : Domaine de Voluceau - Rocquencourt - B.P. 105 - 78153 Le Chesnay Cedex (France)

Éditeur
INRIA - Domaine de Voluceau - Rocquencourt, B.P. 105 - 78153 Le Chesnay Cedex (France)
http://www.inria.fr
ISSN 0249-6399